Advantages of Producing Aromatics from Propene over Ethene Using Zeolite-Based Catalysts

Butolia, Paresh S.; Xi, Xiaoying; Winkelman, Jozef G. M.; Stuart, Marc C. A.; van Akker, Matthijs; Heeres, Andre; Heeres, Hero Jan; Xie, Jingxiu

Published in:
Chemie Ingenieur Technik

DOI:
10.1002/cite.202200080

Publication date:
2022

Advantages of Producing Aromatics from Propene over Ethene Using Zeolite-Based Catalysts

Paresh S. Butolia[1], Xiaoying Xi[1], Jozef G. M. Winkelman[1], Marc C. A. Stuart[2,3], Matthijs van Akker[4], André Heeres[5], Hero Jan Heeres[1], and Jingxiu Xie[1,*]

DOI: 10.1002/cite.202200080

Supporting Information available online

Sustainable production of aromatics, especially benzene, toluene and xylenes (BTX), is essential considering their broad applications and the current global transition away from crude oil utilization. Aromatization of lower olefins, particularly ethene and propene, offers great potential if they are derived from more circular alternative carbon feedstocks such as biomass and waste plastics. This work aims to identify the preferred olefin feed, ethene or propene, for BTX production in a fixed-bed reactor. A commercial H-ZSM-5 (Si/Al = 23) catalyst was used as a reference catalyst, as well as a Ga-ZSM-5 catalyst, prepared by Ga ion-exchange of the H-ZSM-5 catalyst. At 773 K, 1 bar, 45 vol % olefin, 6.75 h^{-1}, propene aromatization over the Ga-ZSM-5 catalyst exhibited higher BTX selectivity of 55 % and resulted in slower catalyst deactivation compared to ethene aromatization.

Keywords: Aromatization, Dehydrogenation, Ethene, Hydrogen-transfer, Propene

Received: May 26, 2022; *revised:* September 30, 2022; *accepted:* October 04, 2022

1 Introduction

Benzene, toluene, xylenes (BTX) are among the most important aromatic hydrocarbons due to their applications in the paint, solvent, plastics and aviation industries [1]. Conventional production of aromatics in the petrochemical industry takes place via catalytic reforming and cracking of fossil-based feedstocks [2]. However, the transition away from non-renewable resources to a circular carbon economy has led to several alternative feedstocks being explored. Lower olefins (C_2–C_4) have garnered significant attention as an attractive solution since the emergence of natural and shale gas [3, 4]. Recently, biomass and plastic wastes have also shown great potential to produce these lower olefins, especially ethene and propene [5].

Considering biomass as an alternative feedstock, lower olefins could be derived directly via catalytic pyrolysis or indirectly using biomass intermediates including alcohols and other oxygenates [6–11]. Catalytic pyrolysis of biomass to aromatics has been shown to produce a significant amount (~15–25 % carbon yield) of ethene and propene as co-products [12–14]. Biomass could also be converted to alcohols and oxygenates such as methanol, ethanol, dimethyl ether, which could be used for the production of C_2–C_3 olefins[15–17]. For instance, dehydration of ethanol/propanol and methanol-to-olefins (MTO) processes have reported selectivity of more than 90 % for ethene and propene [6, 7, 16–18]. Another example is glycerol produced during fermentation or transesterification of biomass which can be

[1]Paresh S. Butolia, Dr. Xiaoying Xi, Dr. Jozef G. M. Winkelman, Prof. Hero Jan Heeres, Dr. Jingxiu Xie
jingxiu.xie@rug.nl
Green Chemical Reaction Engineering, Engineering & Technology Institute Groningen, University of Groningen, Nijenborgh 4, 9747AG Groningen, The Netherlands.

[2]Dr. Marc C. A. Stuart
Groningen Biomolecular Sciences and Biotechnology Institute, University of Groningen, Nijenborgh 7, 9747AG Groningen, The Netherlands.

[3]Dr. Marc C. A. Stuart
Stratingh Institute for Chemistry, University of Groningen, Nijenborgh 4, 9747AG Groningen, The Netherlands.

[4]Matthijs van Akker
BioBTX, Zernikelaan 17, 9747AA Groningen, The Netherlands.

[5]Prof. André Heeres
Research Centre Biobased Economy, Hanze University of Applied Sciences, Zernikeplein 11, 9747AS Groningen, The Netherlands.

used to produce lower olefins (> 85 % selectivity) via hydrodeoxygenation [19, 20]. Along with biomass, plastic waste has also shown potential as a feedstock for the high-volume production of lower olefins. Recently, polymers including high density polyethylene (HDPE), low density polyethylene (LDPE) and polypropylene (PP), have been studied extensively for pyrolysis and their subsequent upgrading to chemicals including BTX [21–23]. Notably, pyrolysis of LPDE, HDPE and PP and other plastic mixtures reported nearly 40 % gas yields of ethene and propene [24–27]. Considering the possibility for large-scale production from these more circular carbon raw materials, the conversion of lower olefins to aromatics could be an important process for a future with circular carbon resources.

Aromatization of lower olefins takes place in the presence of a solid acid catalyst, typically a zeolite, in the temperature range of 673 to 773 K and at atmospheric pressure. Zeolites with the MFI topology, represented by ZSM-5, are most preferred due to their pore dimensions (4.7×4.46×4.46 Å) which are sufficiently large for BTX to be formed and diffuse through and small enough to trap larger aromatic molecules within the pores [28–30]. The olefin aromatization reaction consists of several steps including oligomerization, cracking, cyclization, hydrogen transfer/dehydrogenation reactions based on the hydrocarbon-pool mechanism [31]. Bronsted acid sites (BAS) are considered active sites for all the above-mentioned reaction steps except for dehydrogenation and hydrogen transfer, which are presumed to take place over Lewis acid sites (LAS) [28, 32]. Therefore, BAS is a useful descriptor for activity and stability while LAS has the same function for selectivity towards aromatics. Moreover, the synergistic effect of LAS and BAS in ZSM-5 catalysts is considered critical as it governs the product selectivity and catalyst stability [33].

A high BAS/LAS ratio results in lower BTX selectivity and higher selectivity of gaseous products, so introducing more LAS into the zeolite catalysts has been a popular strategy in catalyst development for the conversion of lower olefins to aromatics. With the incorporation of metal promoters such as Ga, Zn and Ag into the zeolite, new LAS are generated and they act as dehydrogenation centers while also moderating the overall acidity of the catalyst [31, 34–36]. This controls the extent of side reactions such as cracking thus reducing the selectivity of gaseous products while also catalyzing the dehydrogenation reaction, considered to be the rate determining step, thus favoring the aromatic formation via dehydrogenation of cyclic olefins/diolefins. Ga-promoted ZSM-5 catalysts are regarded as one of the most effective aromatization catalysts as they exhibit high conversion of lower hydrocarbons and improved BTX selectivity over commercial ZSM-5 [37–39]. At 773 K, 1 bar, 10 vol % ethene, 3.75 h^{-1}, Ga addition to ZSM-5 improved aromatic selectivity from 12 to 80 %, with a simultaneous decrease in catalytic stability [35]. Under similar temperature and pressure conditions, Ga-promoted catalyst improved the aromatic selectivity from 44 % to 65 % at 773 K and 4.5 h^{-1} when using non-diluted propene [40].

To identify the preferred olefin that could be recycled to attain higher BTX yields from the gaseous product stream of catalytic pyrolysis, this contribution aims to study the impact of using ethene and propene as reactant feed for aromatic production over H-ZSM-5 and Ga-ZSM-5. Importantly, concentrated (45 vol %) ethene and propene feeds were used in reference to the concentration of olefins that is typically present in recycle gas stream from plastic pyrolysis. A H-ZSM-5 commercial zeolite with Si/Al = 23 was used as a reference catalyst. The Ga-modified catalyst was synthesized using ion-exchange and its physicochemical and morphological properties were analyzed and compared with the H-ZSM-5 reference. For both catalysts, experiments with propene led to higher catalytic stability and BTX selectivity at 773 K, thereby presenting a strong case for propene as the preferred olefin to be present in the gas stream of high temperature catalytic pyrolysis of biomass/plastics.

2 Experimental Section

2.1 Catalyst Preparation

NH_4-ZSM-5 (Si/Al=23) was procured from Zeolyst International (CBV 2314), which was then subjected to calcination at 823 K (3 K min^{-1}) for 5 h under static air to obtain the protonated form of ZSM-5 (named H-ZSM-5). To synthesize the Ga-ZSM-5 catalyst using ion-exchange, 0.01 M $Ga(NO_3)_3$ (99.9 % purity; Sigma Aldrich) solution was first mixed with 2 g of H-ZSM-5 [41]. The reactant mixture was heated under constant stirring at 353 K for 6 and then cooled to room temperature and centrifuged to obtain the precipitate. This precipitate was dried at 383 K for 12 h under static air and was later calcined at 823 K for 5 h under static air to obtain the solid catalyst.

2.2 Catalyst Characterization

N_2 adsorption-desorption isotherm measurements were performed at 77 K on Micromeritics ASAP 2420. Pretreatment of the samples was carried out by degassing them under vacuum at 423 K for 12 h before carrying out the N_2 adsorption experiments. The total surface area was calculated using the Brunauer-Emmett-Teller (BET) method. The micropore area and volume were calculated by t-plot method using the adsorption data range of $0.2 < P/P_0 < 0.6$ whereas the total pore volume was obtained at $P/P_0 = 0.99$. Acidity of the catalysts were determined by temperature programmed desorption of ammonia (NH_3-TPD) using a Micromeritics Autochem II 2920. Before the analysis, the sample was subjected to pretreatment at 573 K for 1 h to remove the adsorbed moisture. The sample was then cooled to 393 K and saturated with NH_3 (10 % NH_3/He, 50 mL min^{-1}, 0.5 h). Next, the physically adsorbed NH_3 was

removed by purging He for 30 min and NH_3 was then desorbed from the sample by gradually heating it to 1173 K at a ramping rate of 10 K min^{-1}. X-ray diffraction (XRD) patterns were recorded on D8 Advance Powder Diffractometer (Bruker, Germany) using Cu Kα radiation (λ = 0.154 nm, 40 kV,40 mA). The patterns were recorded at the rate of 2° min^{-1} in the 2θ scanning range of 5–50°. The elemental composition of the catalysts was analyzed using a Malvern Panalytical Epsilon3^{XLE} X-ray fluorescence (XRF) spectrometer. High-resolution transmission electron microscopy (TEM) images were obtained using a Tecnai T20 (FEI, Eindhoven, The Netherlands) electron microscope, operating at 200 kV. Elemental distribution was done in STEM mode on a SDD EDX detector (XmaxT80, Oxford instruments). Before recording the images, the catalyst samples were dispersed in ethanol using ultrasonication bath and its droplets were placed on a Carbon coated Cu grid. Thermogravimetric analysis (TGA) was conducted on spent catalysts using a TGA 4000 (PerkinElmer). For each measurement, 5 mg catalyst was loaded in a ceramic crucible and 30 mL min^{-1} air was used. The temperature was increased from 308 to 1173 K with a heating rate of 20 K min^{-1}.

2.3 Catalyst Evaluation Tests

Calcined catalysts were pressed, crushed and sieved to obtain granules in the range of 212 to 500 µm. 0.2 g catalyst was loaded into a stainless steel fixed-bed reactor (internal diameter of 1 cm) and heated to the reaction temperature at a rate of 5 K min^{-1} under 50 mL min^{-1} N_2 flow. The Ga-ZSM-5 catalysts were subjected to reductive pretreatment under H_2 flow (50 vol % in N_2) at 873 K (5 K min^{-1}) for 1 h. After pretreatment, the reactor was purged with N_2 for 30 min at 873 K and the temperature was set to the reaction temperature. When the reaction temperature was reached, ethene or propene were fed into the reactor (45 vol % in N_2) using Brooks® mass flow controllers to the target weight hourly space velocity (*WHSV*). The liquid products were collected in the cold trap maintained at 263 K and the gaseous stream was analyzed online by a Compact GC (Interscience BV) equipped with two TCD detectors and three capillary columns (Molsieve 5Å, 5 m × 0.32 mm; RT-QBond 3 m × 0.32 mm; RT-QBond 12 m × 0.32 mm). The liquid organic phase was analyzed by an Agilent 8860 GC equipped with an FID detector with a column (Agilent HP-5 30 m × 0.32 mm × 0.25 µm). Conversion and product selectivity were mole-based and were calculated using equation 1 and 2, respectively. The mass balance for all the experiments was in the range of 70–90 %.

$$Conversion(\%) = \frac{n_f^{in} - n_f^{out}}{n_f^{in}} \cdot 100 \quad (1)$$

where n_f^{in} and n_f^{out} indicates moles of feed in the reactant and product stream, respectively.

$$Selectivity(\%) = \frac{n_{c,i}}{n_{ct}} \cdot 100 \quad (2)$$

where $n_{c,i}$ and n_{ct} indicates moles of carbon in product *i* and total moles of carbon in product, respectively.

3 Results and Discussions

The catalysts were characterized using XRF, XRD, TEM, N_2-physisorption and NH_3-TPD. The Ga loading of Ga-ZSM-5 was determined using XRF to be 1.4 wt %. From Fig. 1, the XRD patterns of both H-ZSM-5 and Ga-ZSM-5 showed the characteristic peaks assigned to the MFI topology at their reference positions, i.e., 2θ = 8–9° and 22–25°, suggesting that the crystallinity of the catalyst was not affected upon the addition of Ga. Moreover, no additional diffraction peaks corresponding to Ga_2O_3 were observed, indicating a lack of Ga_2O_3 crystals, which may suggest a homogenous dispersion of Ga ions in the zeolite.

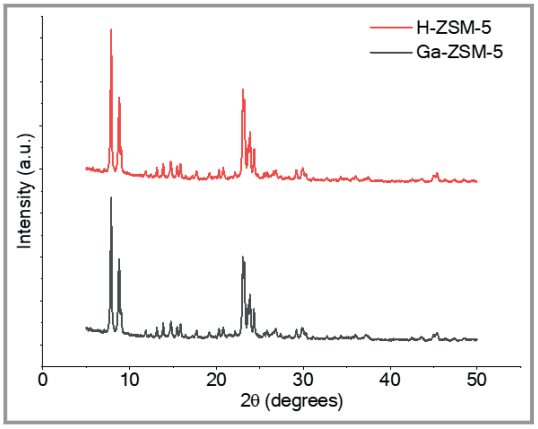

Figure 1. XRD patterns of H-ZSM-5 and fresh Ga-ZSM-5 catalysts.

The Ga dispersion in the Ga-ZSM-5 catalyst was further investigated using STEM-EDX (Fig. 2). The elemental mapping images illustrated uniform distributions of Al, Si and Ga, thereby supporting the XRD finding. Furthermore, the TEM images (Fig. S1, Supporting Information) revealed characteristic lattice fringes of an MFI topology in both Ga-ZSM-5 and H-ZSM-5, thus confirming that the Ga modification did not change the morphology or porosity of the catalyst.

The physical properties and acidities of H-ZSM-5 and Ga-ZSM-5 catalysts are summarized in Tab. 1. Although the Ga modification appeared to decrease the surface area, pore volume and acidity, the differences between H-ZSM-5 and Ga-ZSM-5 were less than 10 %. Referring to Fig. 3, both the catalysts exhibited two similar desorption peaks assigned to weak acid sites, i.e., low temperature (LT) peak (423–523 K) and strong acid sites, i.e., high temperature (HT) peak

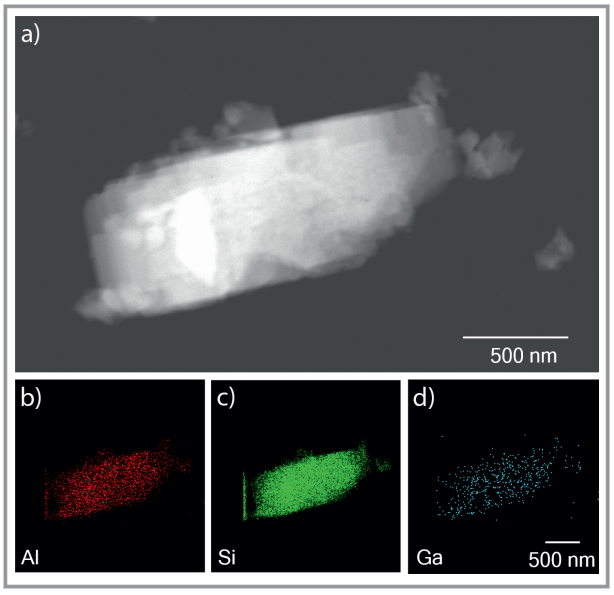

Figure 2. a) STEM image and b–d) elemental distribution in Ga-ZSM-5 catalyst.

(523–723 K). From Tab. S1, the number of strong acid sites were reduced upon Ga modification with a slight shift in the HT peak towards lower temperatures indicating a reduction in strength and number of the strong acid sites respectively. This reduction in strong acid sites may be ascribed to the presence of Ga species replacing the strong acid sites associated with the protons in H-ZSM-5, owing to which the broadening of the peak was observed. Similarly, the number of weak acid sites increased in Ga-ZSM-5 with a small shift in the LT peak towards higher temperature.

Table 1. Physicochemical properties of catalyst samples.

	H-ZSM-5	Ga-ZSM-5
Total surface area[a)] [m^2g^{-1}]	343	321
Micropore area[a)] [m^2g^{-1}]	230	215
External surface area[a)] [m^2g^{-1}]	112	106
Total pore volume[b)] [cm^3g^{-1}]	0.16	0.15
Micropore volume[c)] [cm^3g^{-1}]	0.11	0.10
Total acidity[d)] [mmol g_{cat}^{-1}]	0.91	0.89

a) Calculated by the BET method; b) volume calculated at p/p_0 = 0.99; c) calculated by the t-plot method; d) total acidity determined by NH_3-TPD.

The catalytic performance of the two catalysts were evaluated with an ethene or propene feed at 773 K and 1 bar. The concentration of the olefin reactant at 45 vol % was relatively high in comparison to literature reports in order to mimic the gas stream from plastic pyrolysis. The *WHSV* for both the reactants were selected so as to keep the same

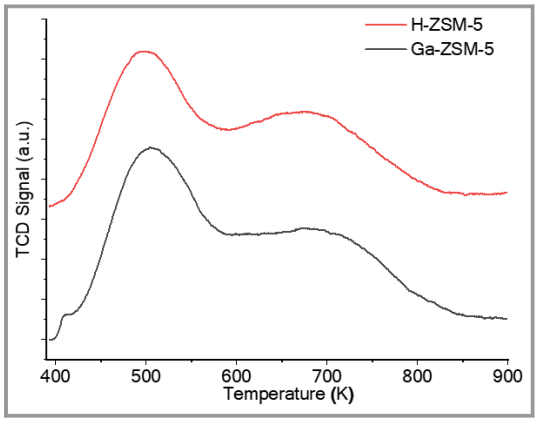

Figure 3. NH_3-TPD profiles for fresh H-ZSM-5 and Ga-ZSM-5.

amount (mass) of carbon available to the catalyst surface at any space time. Fig. 4 provides an overview of olefin conversion and product selectivity as a function of time-on-stream. At 773 K, 1 bar, and 6.75 h^{-1}, the catalyst lifetime of H-ZSM-5 was 8 and 12 h for ethene and propene conversion, respectively (Fig. 4a, 4b). The conversion of propene lasted 1.5 times longer than that of ethene, demonstrating the advantage of propene feed from the perspective of catalytic stability. At identical reaction conditions, the catalyst lifetime of Ga-ZSM-5 was 3 and 6 h for ethene and propene conversion, respectively (Fig. 4c, 4d). The conversion of propene was two times longer than that of ethene, reinforcing the case of propene feed being beneficial for catalytic stability.

In addition to catalytic stability, product selectivity is an important factor. Comparing the product distribution over H-ZSM-5 as depicted in Fig. 4a and 4b, the BTX selectivity was comparable at 48 % for both ethene and propene conversion at the initial period. Selectivity towards other products were also similar at the initial period. However, the product spectrum of H-ZSM-5 changed drastically upon deactivation. At conversion below 20 %, BTX selectivity decreased to 16 % for ethene and 19 % for propene aromatization, respectively. In ethene aromatization, the deactivated H-ZSM-5 mainly produced other aromatics, (8 %), propene (63 %), ethane (6 %) and methane (5 %). In propene aromatization, the deactivated H-ZSM-5 mainly produced other aromatics (6 %), C_4 (48 %) and ethene (23 %).

Referring to Fig. 4c and 4d for the product distribution using Ga-ZSM-5, the BTX selectivity at the initial phase from ethene aromatization was 39 %, compared to 55 % from propene aromatization. This suggests that Ga promotion was more evident in the case of propene aromatization. Both feeds led to 13 % selectivity towards heavier aromatics, including C_9^+ aromatics such as naphthalene, and methyl naphthalene etc. Upon deactivation of the Ga-ZSM-5 catalyst, at conversion level between 10 and 20 %, BTX selectivity was 9 and 13 % for ethene and propene conversion, respectively. Contrary to the product distribution of deacti-

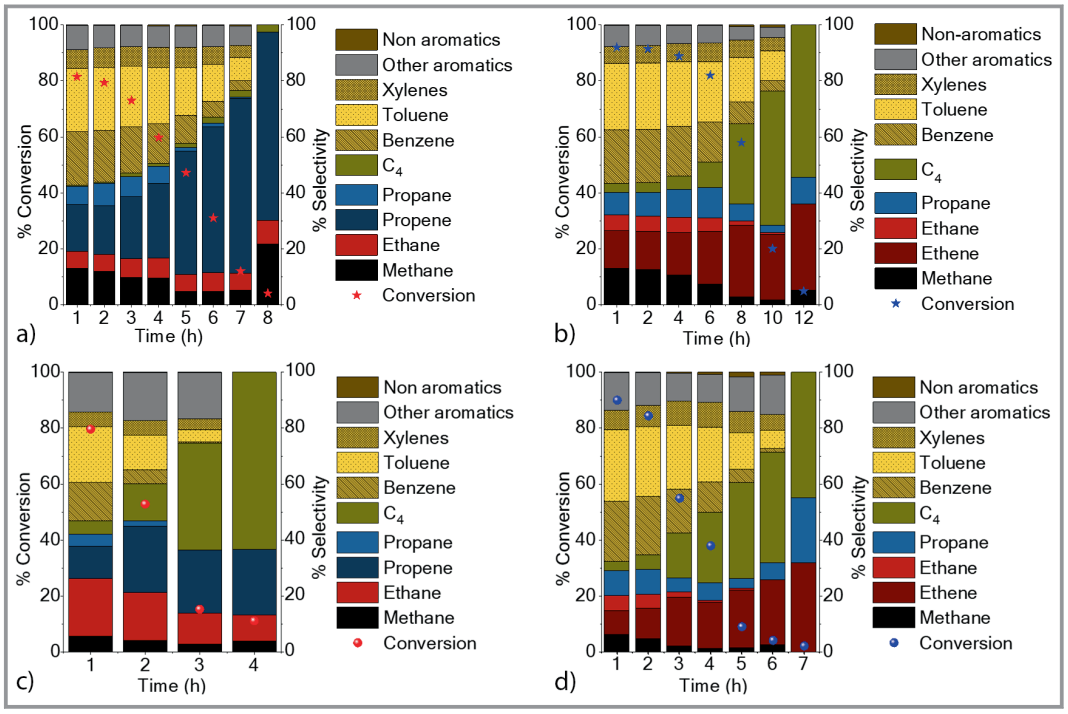

Figure 4. Conversion and product distribution as a function of time-on-stream for conversion of a) ethene, and b) propylene over H-ZSM-5, and c) ethene and d) propene over Ga-ZSM-5 at 773 K, 1 bar, 45 vol % olefin, 6.75 h^{-1}.

vated H-ZSM-5 catalysts, C_4 products were the most significant side-product for both ethene and propene conversion over deactivated Ga-ZSM-5 catalysts.

For both catalysts, deactivation rates were slower during the conversion of propene than of ethene. During aromatization, the catalyst deactivation may proceed over two coking pathways. One of the deactivation routes is via the preferential adsorption of aromatics on the active sites on the catalyst surface compared to olefins, owing to difference in adsorption constants. The lighter aromatics undergo further reaction to yield heavier products, thus hindering the activation of incoming olefins. Notably, the adsorption of aromatics was observed to be stronger with Ga-ZSM-5 than H-ZSM-5 [42]. The other deactivation route is via the deposition of larger molecules or coke precursors inside the pores and channel intersections leading to external blocking of active sites [43, 44]. To determine the amount and nature of the trapped species present in the spent catalysts, thermogravimetric analysis was performed. The loss of weight in the region of 400 to 900 K is attributed to the removal of hydrocarbon and aromatic species trapped in the pores of the zeolites, so called 'soft' coke species, while the weight loss at higher temperatures is due to the removal of polyaromatic 'hard' coke species [45, 46]. From Fig. 5, the 4 % loss in weight of H-ZSM-5 between 400 and 900 K suggest that the deposition of 'soft' coke species was more pronounced in ethene conversion than in propene conversion. The loss in weight after 900 K was higher at 15 %, indicating that there was a higher content of polyaromatic 'hard' coke species which led to catalyst deactivation. The negligible weight loss in the lower temperature region for the spent Ga-ZSM-5 catalysts coupled with a drastic loss in weight, confirmed that the deactivation of Ga-ZSM-5 catalysts was due to deposition of polyaromatic 'hard' coke.

A plausible explanation for the difference in deactivation rate may be derived from the role of these olefins in the hydrocarbon pool mechanism. As illustrated in Fig. 6, the

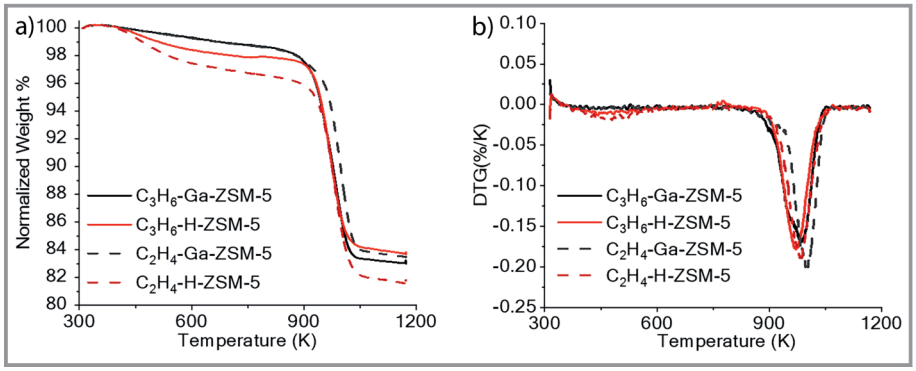

Figure 5. a) TGA and b) DTG curves of spent catalysts after ethene/propene conversion at 773 K, 1 bar and 6.75 h^{-1}.

alkene and arene cycle present within the hydrocarbon pool mechanism are sets of reactions that lead to different products, i.e., aliphatics (mainly olefins) or aromatics [35, 47–49]. In the alkene cycle, olefin oligomerization and cracking take place to yield gaseous products. In the arene cycle, olefin aromatization takes place to yield mainly liquid products. Ethene and propene are known to be predominant products of the arene and alkene cycle, respectively [49–51]. It is also known that at temperatures conducive to aromatic formation (>673 K), lower activity towards oligomerization-cracking reactions results in higher coking rate via formation of coke precursors and polycyclic aromatics [52]. Another possible explanation may be the faster diffusion and stronger adsorption of ethene than propene [53, 54].

The above results present a strong case for propene aromatization instead of ethene aromatization and this may be attributed to the following two reasons. Firstly, there is a stronger bond formation between proton from BAS and propene leading to higher rate of formation of secondary carbenium ions as compared primary carbenium ions from ethene. The secondary carbenium ion formed from propene plays an important role since these ions are readily activated on BAS compared to the primary ones derived from ethene [35]. Secondly, there is a stronger tendency of these protonated intermediates to react with incoming propene and achieve rapid equilibrium with oligomers/olefins formed during transformation [44, 55].

To determine whether our findings on propene being the preferred olefin feed is also true at other reaction temperatures, a similar investigation was performed at a lower reaction temperature of 698 K. From previous studies, olefin aromatization carried out at lower temperature below 673 K mainly resulted in formation of oligomers with traces of aromatics whereas temperatures higher than 773 K led to aromatics formation but also resulted in excess coking [56, 57]. Fig. S3 shows the overview of olefin conversion and product selectivity as a function of time-on-stream at 698 K. The lifetimes of both catalysts in both feeds were longer at 698 K than 773 K, and these correspond well with the lower selectivity towards liquids. In particular, the selectivity towards aromatics decreased at the lower reaction temperature. The analysis of deposited carbon in the spent catalysts tested at 698 K (Fig. S4) was in line with the earlier discussion on deposited carbon in the spent catalysts tested at 773 K (Fig. 5). These results are in agreement with literature, in which the higher temperatures favor aromatization. With an increase in reaction temperature, there is an increase in rate of cyclization and hydrogen transfer for H-ZSM-5. As for Ga-ZSM-5, the notable increase can be attributed to a higher rate of dehydrocyclization, which are usually favored at high temperatures owing to their endothermic nature. Hence, there is a positive correlation between the reaction temperature and the rate of catalyst deactivation. At both 698 K and 773 K, propene conversion over Ga-ZSM-5 exhibited higher BTX selectivity and longer catalyst lifetime (Fig. S5 and S6), thereby strengthening the case of propene aromatization over Ga-ZSM-5 being a viable solution to produce more circular and sustainable BTX in the future.

4 Conclusion

Ethene and propene aromatization were studied using a commercial H-ZSM-5 (Si/Al = 23) and a Ga-ZSM-5 catalyst. Ga modification of the commercial H-ZSM-5 catalyst was performed with the ion-exchange approach and the Ga loading was determined to be 1.4 wt % using XRF. Both XRD and (S)TEM-EDX indicated a homogenous dispersion of Ga species. NH_3-TPD used to probe acidity in the catalysts showed a slight decrease in both number and strength of BAS upon Ga modification. At 773 K, 1 bar, 45 vol % olefin feed for Ga-ZSM-5, propene aromatization led to improved catalyst lifetime and BTX selectivity compared to ethene. Thus, propene appears to be a more promising feedstock compared to ethene for BTX production. Propene can also aid in improving the overall aromatic yield from biomass and waste plastics if it can be selectively produced in the recycle gas stream from catalytic pyrolysis of the respective feedstocks and made to undergo subsequent conversion processes.

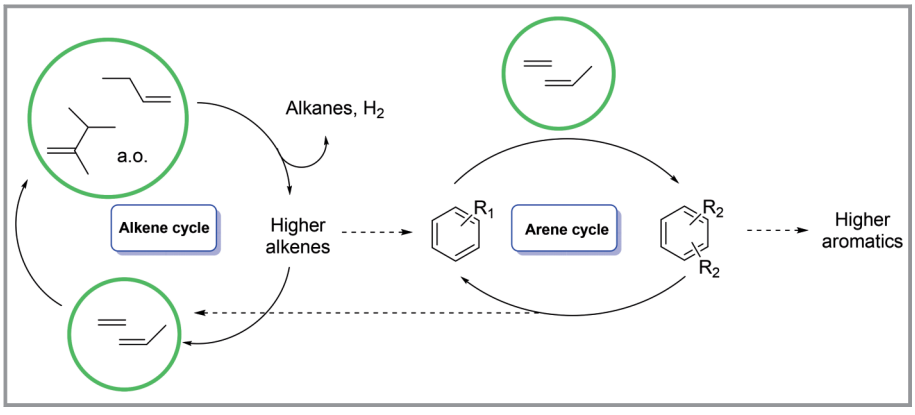

Figure 6. Example of dual-hydrocarbon cycle mechanism for ethene and propene (a. o.: amongst others).

Supporting Information

Supporting Information for this article can be found under DOI: https://doi.org/10.1002/cite.202200080.

BioBTX, an important partner in this research, is acknowledged for financial support and fruitful discussion. Leon Rohrbach is acknowledged for analytical support; Henk van de Bovenkamp and Erwin Wilbers are acknowledged for technical support.

Symbols used

g_{cat}	[g]	Mass of catalyst
L	[Å]	Length
T	[K]	Temperature
TOS	[h]	Time-on-stream
V	[vol %]	Percentage by volume
W	[wt %]	Percentage by weight
$WHSV$	[h^{-1}]	Weight hourly space velocity

Greek letters

θ	[°]	Incident angle
λ	[nm]	Wavelength

Abbreviations

BAS	Bronsted acid sites
BET	Brunauer-Emmett-Teller
BTX	Benzene, Toluene, Xylenes
DTG	Differential thermogravimetry
EDX	Energy dispersive X-ray
FID	Flame ionization detector
GC	Gas chromatography
HDPE	High density polyethylene
HT	High temperature
LAS	Lewis acid sites
LDPE	Low-density polyethylene
LT	Low temperature
MFI	Mobil-type five
PP	Polypropylene
SDD	Silicon drifts detector
TCD	Thermal conductivity detector
TEM	Transmission electron microscopy
TGA	Thermogravimetric analysis
TOS	Time-on-stream
TPD	Temperature programmed desorption
WHSV	Weigh hourly space velocity
XRF	X-ray fluorescence
ZSM-5	Zeolite Socony Mobil-5

References

[1] H. A. Wittcoff, B. G. Reuben, J. S. Plotkin, *Industrial Organic Chemicals*, Wiley, Hoboken, NJ **2012**.
[2] G. Busca, *Energies* **2021**, *14 (13)*, 461. DOI: https://doi.org/10.3390/en14134061
[3] I. Amghizar, L. A. Vandewalle, K. M. Van Geem, G. B. Marin, *Engineering* **2017**, *3 (2)*, 171–178. DOI: https://doi.org/10.1016/j.Eng.2017.02.006
[4] P. C. A. Bruijnincx, B. M. Weckhuysen, *Angew. Chem., Int. Ed.* **2013**, *52 (46)*, 11980–11987. DOI: https://doi.org/10.1002/anie.201305058
[5] A. Eschenbacher, R. J. Varghese, M. S. Abbas-Abadi, K. M. Van Geem, *Chem. Eng. J.* **2022**, *428*, 132087. DOI: https://doi.org/10.1016/j.cej.2021.132087
[6] M. Zhang, Y. Yu, *Ind. Eng. Chem. Res.* **2013**, *52 (28)*, 9505–9514. DOI: https://doi.org/10.1021/ie401157c
[7] A. W. Lepore et al., *Ind. Eng. Chem. Res.* **2017**, *56 (15)*, 4302–4308. DOI: https://doi.org/10.1021/acs.iecr.7b00592
[8] Y. Zhi et al., *J. Am. Chem. Soc.* **2015**, *137 (50)*, 15781–15794. DOI: https://doi.org/10.1021/jacs.5b09107
[9] M. Yang et al., *Bioresour. Technol* **2019**, *273*, 77–85. DOI: https://doi.org/10.1016/j.biortech.2018.11.005
[10] I. A. Bakare et al., *Fuel* **2018**, *211*, 18–26. DOI: https://doi.org/10.1016/j.fuel.2017.08.117
[11] S. He et al., *Fuel Process. Technol.* **2021**, *221*, 106944. DOI: https://doi.org/10.1016/j.fuproc.2021.106944
[12] X. Dong et al., *RSC Adv.* **2013**, *3 (48)*, 25780–25787. DOI: https://doi.org/10.1039/c3ra43850c
[13] K. Wang, P. A. Johnston, R. C. Brown, *Bioresour. Technol.* **2014**, *173*, 124–131. DOI: https://doi.org/10.1016/j.biortech.2014.09.097
[14] W. Huang et al., *Bioresour. Technol.* **2012**, *121*, 248–255. DOI: https://doi.org/10.1016/j.biortech.2012.05.141
[15] S. Park et al., *J. Catal.* **2014**, *319*, 265–273. DOI: https://doi.org/10.1016/j.jcat.2014.09.002
[16] D. Fan, D.-J. Dai, H.-S. Wu, *Materials* **2012**, *6 (1)*, 101–115. DOI: https://doi.org/10.3390/ma6010101
[17] Y. A. Treger, V. N. Rozanov, *Rev. J. Chem.* **2016**, *6 (1)*, 83–123. DOI: https://doi.org/10.1134/s2079978016010039
[18] P. Tian, Y. Wei, M. Ye, Z. Liu, *ACS Catal.* **2015**, *5 (3)*, 1922–1938. DOI: https://doi.org/10.1021/acscatal.5b00007
[19] V. Zacharopoulou, A. Lemonidou, *Catalysts* **2017**, *8 (1)*, 2. DOI: https://doi.org/10.3390/catal8010002
[20] V. Zacharopoulou, E. S. Vasiliadou, A. A. Lemonidou, *ChemSusChem* **2018**, *11 (1)*, 264–275. DOI: https://doi.org/10.1002/cssc.201701605
[21] A. Inayat et al., *Fuel* **2022**, *314*, 123071. DOI: https://doi.org/10.1016/j.fuel.2021.123071
[22] N. Kiran Ciliz, E. Ekinci, C. E. Snape, *Waste Manage.* **2004**, *24 (2)*, 173–181. DOI: https://doi.org/10.1016/j.wasman.2003.06.002
[23] P. Das, P. Tiwari, *Waste Manage.* **2018**, *79*, 615–624. DOI: https://doi.org/10.1016/j.wasman.2018.08.021
[24] P. J. Donaj, W. Kaminsky, F. Buzeto, W. Yang, *Waste Manage.* **2012**, *32 (5)*, 840–846. DOI: https://doi.org/10.1016/j.wasman.2011.10.009
[25] P. Kannan, A. Al Shoaibi, C. Srinivasakannan, *Energy Fuels* **2014**, *28 (5)*, 3363–3366. DOI: https://doi.org/10.1021/ef500516n
[26] M. Artetxe et al., in *Advanced Technology for the Conversion of Waste Into Fuels and Chemicals* (Eds: A. Khan et al.), Woodhead Publishing, Sawston **2021**.
[27] M. Artetxe et al., *Ind. Eng. Chem. Res.* **2013**, *52 (31)*, 10637–10645. DOI: https://doi.org/10.1021/ie4014869
[28] V. Hulea, *ACS Catal.* **2018**, *8 (4)*, 3263–3279. DOI: https://doi.org/10.1021/acscatal.7b04294

[29] A. Mehdad, R. F. Lobo, *Catal. Sci. Technol* **2017**, *7 (16)*, 3562–3572. DOI: https://doi.org/10.1039/c7cy00890b
[30] C. M. Lok, J. Van Doorn, G. Aranda Almansa, *Renewable Sustainable Energy Rev.* **2019**, *113*, 109248. DOI: https://doi.org/10.1016/j.rser.2019.109248
[31] X. Chen et al., *Chin. J. Catal.* **2015**, *36 (6)*, 880–888. DOI: https://doi.org/10.1016/s1872-2067(14)60289-8
[32] A. Bonnin et al., *Appl. Catal., A* **2021**, *611*, 117974. DOI: https://doi.org/10.1016/j.apcata.2020.117974
[33] J. A. Biscardi, G. D. Meitzner, E. Iglesia, *J. Catal.* **1998**, *179 (1)*, 192–202. DOI: https://doi.org/10.1006/jcat.1998.2177
[34] M. F. Hsieh et al., *ChemCatChem* **2017**, *9 (9)*, 1675–1682. DOI: https://doi.org/10.1002/cctc.201700192
[35] E. A. Uslamin et al., *Catal. Sci. Technol.* **2020**, *10 (9)*, 2774–2785. DOI: https://doi.org/10.1039/c9cy02108f
[36] H. Coqueblin et al., *Catal. Today* **2017**, *289*, 62–69. DOI: https://doi.org/10.1016/j.cattod.2016.08.006
[37] P. Qiu, J. H. Lunsford, M. P. Rosynek, *Catal. Lett.* **1998**, *52 (1/2)*, 37–42. DOI: https://doi.org/10.1023/a:1019046714762
[38] V. R. Choudhary, P. Devadas, S. Banerjee, A. K. Kinage, *Microporous Mesoporous Mater.* **2001**, *47 (2–3)*, 253–267. DOI: https://doi.org/10.1016/s1387-1811(01)00385-7
[39] V. R. Choudhary, D. Panjala, S. Banerjee, *Appl. Catal., A* **2002**, *231 (1–2)*, 243–251. DOI: https://doi.org/10.1016/s0926-860x(02)00061-3
[40] J. Park, W. Y. Lee, H.-S. Hahm, *Korean J. Chem. Eng.* **2002**, *19 (3)*, 411–416. DOI: https://doi.org/10.1007/bf02697148
[41] A. Heeres et al., *ACS Sustainable Chem. Eng.* **2018**, *6 (3)*, 3472–3480. DOI: https://doi.org/10.1021/acssuschemeng.7b03728
[42] C. R. Bayense, J. H. C. van Hooff, *Appl. Catal., A* **1991**, *79 (1)*, 127–140. DOI: https://doi.org/10.1016/0926-860x(91)85011-l
[43] A. Samanta et al., *Ind. Eng. Chem. Res.* **2017**, *56 (39)*, 11006–11012. DOI: https://doi.org/10.1021/acs.iecr.7b02095
[44] D. B. Lukyanov, N. S. Gnep, M. R. Guisnet, *Ind. Eng. Chem. Res.* **2002**, *33 (2)*, 223–234. DOI: https://doi.org/10.1021/ie00026a008
[45] Y. Li et al., *Fuel* **2017**, *189*, 23–31. DOI: https://doi.org/10.1016/j.fuel.2016.10.047
[46] M. Díaz et al., *Appl. Catal., B* **2021**, *291*, 120076. DOI: https://doi.org/10.1016/j.apcatb.2021.120076
[47] I. Yarulina et al., *Nat. Catal.* **2018**, *1 (6)*, 398–411. DOI: https://doi.org/10.1038/s41929-018-0078-5
[48] M. Bjorgen et al., *J. Catal.* **2007**, *249 (2)*, 195–207. DOI: https://doi.org/10.1016/j.jcat.2007.04.006
[49] S. Svelle et al., *J. Am. Chem. Soc.* **2006**, *128 (46)*, 14770–14771. DOI: https://doi.org/10.1021/ja065810a
[50] S. Svelle, U. Olsbye, F. Joensen, M. Bjørgen, *J. Phys. Chem. C* **2007**, *111 (49)*, 17981–17984. DOI: https://doi.org/10.1021/jp077331j
[51] K. Lee, S. B. Hong, *ACS Catal.* **2019**, *9 (12)*, 10640–10648. DOI: https://doi.org/10.1021/acscatal.9b03434
[52] E. Epelde et al., *Microporous Mesoporous Mater.* **2014**, *195*, 284–293. DOI: https://doi.org/10.1016/j.micromeso.2014.04.040
[53] E. A. Redekop, A. Lazzarini, S. Bordiga, U. Olsbye, *J. Catal.* **2020**, *385*, 300–312. DOI: https://doi.org/10.1016/j.jcat.2020.03.020
[54] P. Cnudde et al., *J. Am. Chem. Soc.* **2020**, *142 (13)*, 6007–6017. DOI: https://doi.org/10.1021/jacs.9b10249
[55] G. Spoto et al., *J. Chem. Soc., Faraday Trans.* **1994**, *90 (18)*, 2827–2835. DOI: https://doi.org/10.1039/ft9949002827
[56] D. S. Fernandes, C. O. Veloso, C. A. Henriques, *Catal. Lett.* **2019**, *150 (3)*, 738–752. DOI: https://doi.org/10.1007/s10562-019-02954-w
[57] X. Huang, D. Aihemaitijiang, W.-D. Xiao, *Chem. Eng. J.* **2015**, *280*, 222–232. DOI: https://doi.org/10.1016/j.cej.2015.05.124

